Absorption spectrum (380–700 nm) of pure water. II. Integrating cavity measurements

Robin M. Pope and Edward S. Fry

Definitive data on the absorption spectrum of pure water from 380 to 700 nm have been obtained with an integrating cavity technique. The results are in good agreement with those recently obtained by our group with a completely independent photothermal technique. As before, we find that the absorption in the blue is significantly lower than had previously been generally believed and that the absorption minimum is at a significantly shorter wavelength, i.e., 0.0044 ± 0.0006 m^{-1} at 418 nm. Several spectroscopic features have been identified in the visible spectrum to our knowledge for the first time.

Key words: Absorption, integrating cavity, water, ocean water, spectroscopy.

1. Introduction

Extensive references to the literature on the spectral absorption of pure water are available.[1,2] These indicate wide variability in observed values and considerable uncertainty as to the actual values. We have recently made measurements by two completely independent approaches: (1) a photothermal probe beam deflection technique that is discussed in the previous paper[3] and (2) an integrating cavity technique that is discussed in this paper. Both approaches are effectively independent of scattering effects at levels that might be observed in ocean water. Although they are completely different approaches, they give results that are in good agreement and provide critical evidence that our new absorption data in the blue are more reliable than previously published data. The integrating cavity technique is, however, significantly simpler to implement.

These two approaches actually involve the measurement of different physical quantities. In the photothermal technique, only that fraction of light energy that is removed from the incident light field and converted into thermal energy is measured. In the integrating cavity technique, all the light energy that is removed from the incident light field is measured. In the case of pure water in the visible region of the spectrum, these are essentially the same since fluorescence and photochemical processes are negligible.[4] The main common denominator of the research that we describe in this paper and in the previous paper is the use of the same source of pure water.

The integrating cavity absorption meter (ICAM) permits the measurement of very small optical absorption coefficients (0.001 m^{-1}), virtually independent of scattering effects in the sample. Briefly, the sample is isotropically illuminated in a cavity whose walls have a very high diffuse reflectivity, typically >99%. The optical energy lost in the cavity is proportional to the absorption coefficient of the sample and can be monitored by using optical fibers to sample the irradiance entering and leaving the cavity. The negligible effects of scattering are a result of the isotropic illumination and the fact that elastic scattering does not remove any energy from the cavity. The theoretical basis, working equations, and effects of scattering particles on the absorption coefficients measured in an ICAM have been previously reported.[5] The major ICAM innovation implemented here is a method for its absolute calibration.

We have used the ICAM to measure the absorption spectrum of pure water in the 380–700-nm wavelength region. Our results indicate that the absorption of pure water in the 420-nm region is more than a factor of 3 lower than previously accepted values.[6] Our measurements confirm the observations of the

When this research was performed both authors were with the Department of Physics, Texas A&M University, College Station, Texas 77843-4242. R. M. Pope is now with the U.S. Army, Fort Belvoir, Virginia 22060-5823. E. S. Fry is also with the Texas Laser Laboratory, Houston Advanced Research Center, The Woodlands, Texas 77381.

Received 5 March 1997; revised manuscript received 17 July 1997.

0003-6935/97/338710-14$10.00/0

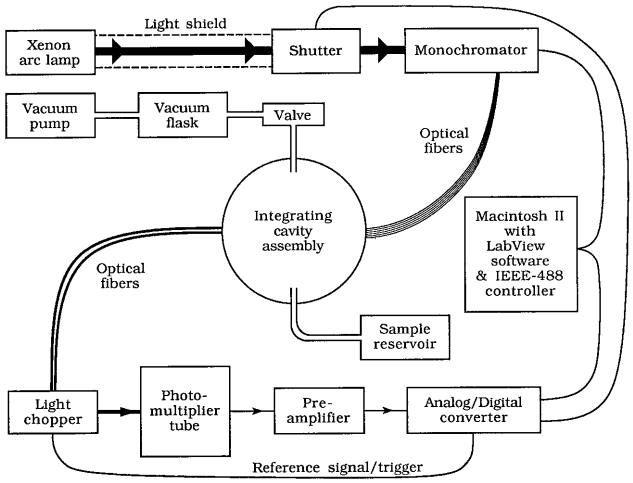

Fig. 1. Block diagram of the ICAM system.

seventh and eighth harmonics of the O–H stretching mode that were first reported in the research discussed in the previous paper.[3,7] We have further identified structures in the absorption spectrum of pure water that are due to combinations of the fundamental frequency of the scissors mode with harmonics of the O–H stretching mode.

2. Description of the Integrating Cavity Absorption Meter Instrumentation

A prototype version of the ICAM has been previously described.[5] Figure 1 is a block diagram of the ICAM system as configured for the present measurements. Two substantive changes from the previous description are the following: (1) input wavelength selection with a monochromator instead of a set of interference filters and (2) enhancement of some signal measurement and processing functions. Full documentation of the instrument configuration used for these measurements is available[8]; it is briefly reviewed here.

The light source is a 150-W ozone-free xenon arc lamp.[9] The monochromator has UV-grade optics and a reversible two-grating mount[10]; its nominal bandwidth of 1.9 nm is based on an average 600-μm slit width (the monochromator dispersion is 3.2 nm mm^{-1}). An electromagnetic camera shutter with a 45-mm-diameter opening is attached to the cover plate on the entrance slit of the monochromator.[11] By closing this shutter, background signals that are due to stray light and photomultiplier tube dark current can be measured. The light path from the arc lamp to the shutter is shielded from dust, stray light, and unintentional obstructions. A custom fiber-optic assembly collects light from the exit slit of the monochromator and delivers it to the integrating cavity assembly. This fiber assembly consists of six silica-core, silica-clad optical fibers, each having a 600-μm core diameter and a 1.0-mm nominal overall diameter; at the monochromator end, the six fibers are arranged in a vertical linear array that collects light over the height of the exit slit.

The integrating cavity assembly consists of two concentric integrating cavities, a quartz-glass sample cell with inlet and outlet ports, and optical fibers. Cross sections of the integrating cavity assembly parallel and transverse to the Z axis are shown in Figs. 2(a) and 2(b), respectively. Viewed along the Z axis [Fig. 2(b)], the outer cavity has a hexagonal cross section with 11 cm between inside faces. Its wall is made of interlocking Spectralon[12] plates 1.27 cm thick and 25.4 cm high. The inner cavity is a 16-cm-high Spectralon cylinder with a 10-cm outside

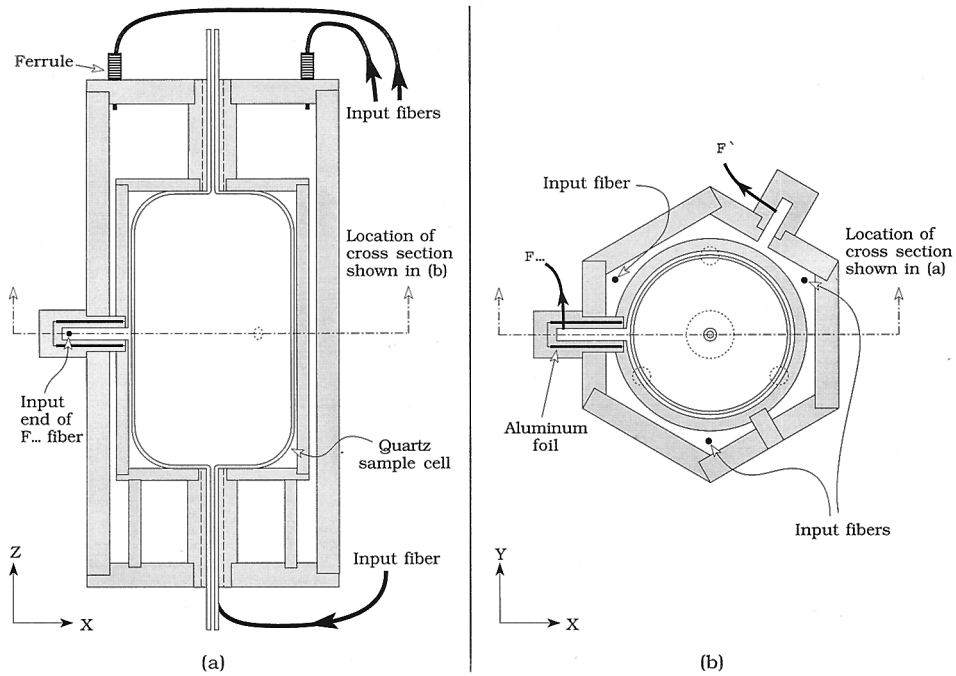

Fig. 2. Cross sections of the integrating cavity (a) perpendicular to the Y axis at the location indicated in (b) and (b) perpendicular to the Z axis at the location indicated in (a).

diameter and 6.3-mm-thick walls and end caps. The inner cavity is held at the midpoint of the outer cavity by a Spectralon tube centered on the axis at each end of the cavity; the tubes are 5 cm long with a 2.54-cm outside diameter and an 8-mm inside diameter. Additional support and stability are provided by three Spectralon dowels at each end of the cavity. The dowels are 8 mm in diameter and 5 cm long; they are symmetrically located about the axis on an 8.6-cm-diameter circle. The three dowels at one end of the cavity are offset by 60° from those at the other end.

Light is supplied to the cavity through the six fibers of the fiber-optic assembly. Three sections of hypodermic tubing pass through each end cap and terminate in the outer cavity; these support and shield the six fiber tips. The three fibers passing through each end cap are 120° apart on a 6.4-cm-diameter circle, and those at one end are offset by 60° with respect to those at the other end. The arbitrary choice of six input fibers provided direct illumination of the entire outer cavity; however, the diffuse reflectivity of the Spectralon is so high that even one fiber might have been sufficient to provide the required uniform illumination of the sample volume.

The inner cavity is lined with a quartz cell that tapers into quartz capillary tubing at each end. This quartz sample cell permits the exchange of samples without opening the cavities and also prevents direct contact between the Spectralon and the sample. The sample cell used in this study has a 0.6-l capacity. Its outside surface is heavily frosted in order to reduce refractive-index effects as light enters the cell through the quartz–air interface.[13]

The outward irradiance incident on the inside wall of the inner cavity is F_0; similarly, the outward irradiance on the inside wall of the outer cavity is F_1. Each irradiance is measured with two optical fibers positioned at the midpoint of the cylinder axis and separated by 120° in the X–Y plane as shown in Fig. 2(b). Both are silica-core, silica-clad optical fibers with an 800-μm core diameter. Black vinyl tubing is used to shield the fibers between the points where they exit the outside cavity wall and their termination points at the photomultiplier tube.

To sample F_0, a 6.3-mm hole is drilled in the wall of the inner cavity. A Spectralon cup with a 6.3-mm inside diameter and a 1.6-mm-thick wall is inserted through the outer cavity wall and into a recess formed in the outside of the inner cavity wall; the recess centers the cup on the 6.3-mm hole. An optical fiber placed near the back of the cup as shown in Fig. 2(b) provides a light sample proportional to F_0. An aluminum foil shield prevents the radiance in both the outer cavity and the inner cavity wall from penetrating the walls of the cup. To prevent this foil shielding from appreciably perturbing either radiance, it is surrounded by a second Spectralon cup with a 9.5-mm inside diameter and a 4.8-mm-thick wall. To sample F_1, we inserted a second Spectralon cup with an identical optical fiber into the outer cavity wall as shown in Fig. 2(b); of course, no foil shielding is needed here.

The integrating cavity assembly is enclosed in a black Plexiglas box to shield the cavity assembly from external light sources. This Plexiglas enclosure has ports for the two tubes on the quartz sample cell, for the six input optical fibers, and for the two detector optical fibers. Gaps between the ports and the components passing through them are sealed with black silicone rubber. The quartz tube passing through the port at the top of the enclosure is formed into a helix, painted flat black, and shielded with black vinyl to suppress external light entry into the sample cell. The quartz tube at the bottom passes directly from the enclosure into a light tight compartment beneath the cavity assembly; it is attached to a Teflon tube that is inserted into a flask or bottle that serves as a reservoir for the sample to be measured. This compartment shields the sample container and the Teflon tubing from external light sources.

The F_0 and F_1 fibers pass through a 2.54-cm port in the wall of the enclosure. This port is sealed by an O-ring to an adjacent compartment containing the detector-chopper assembly. A single Burle 4840 photomultiplier tube is used to measure both the F_0 and F_1 irradiance. This is accomplished by a custom-made light chopper that blocks the light from the F_1 fiber at a 100-Hz rate; the photomultiplier output current is then a square wave whose low value is proportional to F_0 and whose high value is proportional to $F_1 + F_0$. A preamplifier converts the current from the photomultiplier tube to a voltage signal, and an analog-to-digital converter (IOtech Incorporated Model ADC488/16A) provides a digital output signal with 16-bit resolution for as many as 100,000 samples/s. Thus there are approximately 1000 data points for each period of the 100-Hz signal produced by the detector-chopper assembly.

To minimize handling them, the pure-water samples are siphoned into the sample cell by the vacuum system shown in the block diagram (Fig. 1). A weak vacuum (5–10 psi) siphons the sample out of the reservoir at the bottom of the cavity assembly, through the Teflon tubing, and into the sample cell in the ICAM. A taper in the bottom and top of the sample cell ensures complete drainage or filling of the sample cell and prevents air trapping at the top. The temperature of the water in the reservoir was stable at 22 °C; variations never exceeded ±1 °C during the pure-water measurements.

Data acquisition, instrument control, and signal processing and analysis are accomplished with the LabVIEW programming language from National Instruments.

3. Theoretical Background

We have shown that the power absorbed in a sample illuminated with a homogeneous and isotropic radiance distribution can be written as[5]

$$P_{\text{abs}} = 4aVF_0, \tag{1}$$

where V is the sample volume, F_0 is the outward normal component of the vector irradiance from

within the sample at its surface, and a is the absorption coefficient of the sample. By conservation of energy, the power entering the sample volume must equal the power leaving the volume plus the power absorbed:

$$P_{\text{in}} = P_{\text{out}} + P_{\text{abs}}, \tag{2}$$

which combined with Eq. (1) gives

$$P_{\text{in}} = P_{\text{out}} + 4aVF_0. \tag{3}$$

We can write the power in and the power out in terms of each irradiance, F_0 and F_1. The power entering the sample will be proportional to F_1. The power exiting the sample, through the Spectralon wall, exit ports, detectors, etc. will be proportional to F_0. If we designate the proportionality constants as K_1 and K_0, respectively, the energy conservation equation becomes

$$K_1F_1 = K_0F_0 + 4aVF_0. \tag{4}$$

As described above, each irradiance, F_0 and F_1, is sampled by optical fibers and detected by a photomultiplier to produce corresponding signal voltages S_0 and S_1. Since these voltages depend on the spectral responses of the detector and fiber optics, Eq. (4) can be rewritten as

$$C_1S_1 = C_0S_0 + 4aVS_0. \tag{5}$$

The proportionality constants C_0 and C_1 replacing K_0 and K_1 include the additional dependencies on the fiber and detector spectral responses. Dividing Eq. (5) by C_1S_0, replacing S_1/S_0 by S, and replacing C_0/C_1 by C_0' gives a simple equation that is linear in S, a, and V:

$$S = \frac{4}{C_1}aV + C_0'. \tag{6}$$

Solving for the absorption coefficient a gives

$$a = \frac{C_1}{4V}(S - C_0') \equiv C_1'(S - C_0'). \tag{7}$$

This simple relation is the working equation for the ICAM. Its implementation requires determination of two calibration constants: the overall normalization constant C_1' and the offset constant C_0'; of course, both constants depend on the wavelength. Two partial derivatives of these relations will be useful. From Eqs. (6) and (7) we have

$$\left.\frac{\partial S}{\partial V}\right|_a = \frac{4}{C_1}a, \tag{8}$$

$$\left.\frac{\partial a}{\partial S}\right|_V = \frac{C_1}{4V}, \tag{9}$$

respectively. Thus $\partial S/\partial V$ is proportional to the absorption coefficient a.

4. Calibration

For an ideal cavity and at a fixed wavelength, C_1 and C_0' are constants (independent of a). When the cavity is empty corresponding to $a = 0$, the signal is denoted by S_E; hence, from Eq. (7) the signal offset C_0' for an ideal cavity is given by $C_0' = S_E$. The other constant $C_1/4V$ can be determined by measuring the signal S for a calibration solution whose absorption coefficient a is accurately known and then by using Eq. (7).

Unfortunately, the irradiance in an experimental realization of the ICAM is perturbed by leakage of optical energy from the cavity in the vicinity of the holes in it; there is a hole for the detector at the cavity midpoint, and there is one at its top and one at its bottom for sample cell access. In addition, index of refraction effects on the outgoing radiance in the vicinity of the detector will systematically alter the cavity full and cavity empty signals. These perturbations lead to an effective sample volume that differs from the actual sample volume. Furthermore, their effect on the outgoing irradiance F_0 will, in general, depend on the sample absorption; this dependence must be identified and isolated in order to calibrate the ICAM. In analogy with Eq. (7), a new overall normalization constant C_1'' and a new offset constant C_0'' will be defined for our practical realization of the ICAM.

A. Determination of the Offset Calibration Constant C_0''

Equation (6) indicates that for an ideal cavity, the y intercept in a plot of signal S versus sample volume V for a sample of constant, albeit unknown, absorption should just be the offset C_0', where both C_0' and S depend on the wavelength. Therefore the volume of water in the sample cell was increased from empty to full (0.6 l) by adding water (not ultrahigh purity) in increments of 0.025 l; and at each increment in volume, S was measured at 2.5-nm intervals over the 380–750-nm spectral range. For each wavelength interval, $S(V)$ was extracted from these data; Fig. 3 shows examples at six wavelengths. Clearly, the results are not as simple as suggested by Eq. (6) for an ideal cavity; there is a shift in S when the cavity is approximately half full (i.e., at $\approx$0.325 l, corresponding to a water level at the position of the F_0 detector), and there are systematic shifts in S for the cavity empty $S(0.0) \equiv S_E$ and full $S(0.6) \equiv S_F$. The latter are due to effects of the perturbations on the radiance distributions at the bottom and top of the cell, respectively. Figure 4(a) shows a simulation of a typical data set at some wavelength and defines the three systematic signal shifts: $s_0(\lambda)$ is the signal shift at the center of the cell, $s_1(\lambda)$ is the cavity-empty shift, and $s_2(\lambda)$ is the cavity-full shift; all three are defined as positive as shown in Fig. 4(a).

The values of s_0, s_1, s_2, and $\partial S/\partial V$ must be determined by fitting straight lines to the $S(V)$ data at each wavelength; since S_E, $S(0.325)$, and S_F exhibit systematic deviations, these three data points are excluded. Now the slope $\partial S/\partial V$ of the data is the same

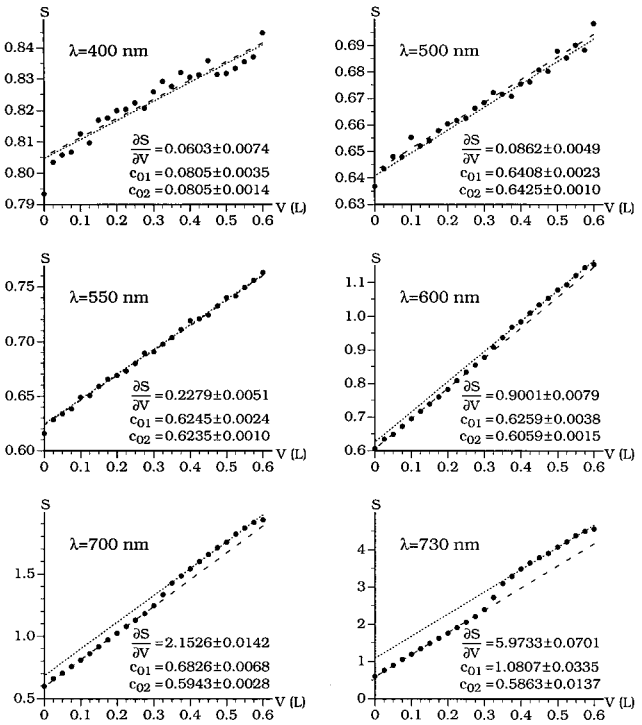

Fig. 3. Examples of the signal S as a function of the volume V (liters) at six wavelengths. Also shown are the two straight-line fits to the data, the value of their slope, the two y intercepts, and the standard deviations.

above and below the midpoint, so we define a fitting function of the form

$$f(V) = c_{01}\Theta(V - 0.325) + c_{02}\Theta(0.325 - V) + V\frac{\partial S}{\partial V}, \quad (10)$$

where $\Theta(\ldots)$ is the Heaviside unit step function; the graph in Fig. 4(a) shows $f(V)$. The function $f(V)$ is fitted to the $S(V)$ data (less the three points) with a linear least-squares fitting procedure to determine the three fitting parameters c_{01}, c_{02}, and $\partial S/\partial V$. At each wavelength, the shifts s_0, s_1, and s_2 are given in terms of the fitted parameters by $s_0 = c_{01} - c_{02}$; $s_1 = c_{02} - S_E$; and $s_2 = S_F - c_{01} - 0.6^*\partial S/\partial V$. For the six data sets in Fig. 3, we show the two fitted straight

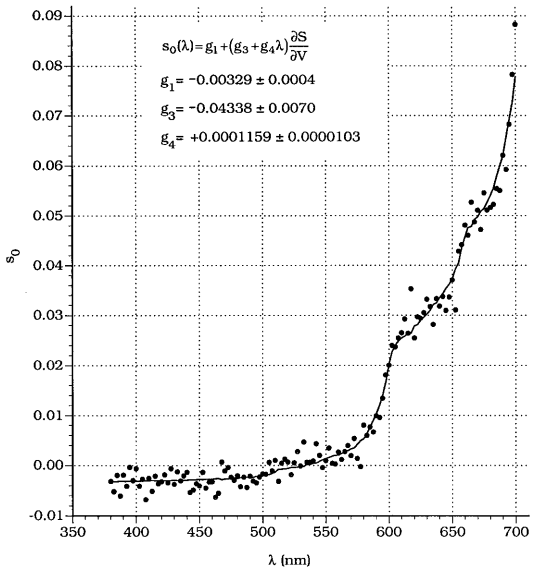

Fig. 5. Offset s_0 as a function of λ (nanometers). The solid curve is a least-squares fit to the data points; the slight irregularities are due to statistical fluctuations in the $\partial S/\partial V$ data.

lines together with the fitting parameters and their standard deviations; note, for example, the change in sign of s_0.

Next we consider the wavelength dependence of the three signal shifts $s_i(\lambda)$ ($i = 0, 1, 2$) we have just evaluated. As indicated in Fig. 4(b), each can, in general, be considered a linear combination of a pure signal change δS_i and an effective volume change δV_i:

$$s_i = \delta S_i + \delta V_i \frac{\partial S}{\partial V} = \delta S_i + \delta V_i \frac{4}{C_1} a, \quad (11)$$

where we have used Eq. (8) to replace $\partial S/\partial V$. As expected from the discussion at the beginning of this section, Eq. (11) shows that s_i can depend on the absorption coefficient a.

Although it will not be needed, a fit to the $s_0(\lambda)$ data is instructive. The fit clearly shows the dependence on a and demonstrates the procedure in a simple case. The offset at the center of the cell is obtained from $s_0(\lambda) = c_{01}(\lambda) - c_{02}(\lambda)$ and is shown in Fig. 5; the

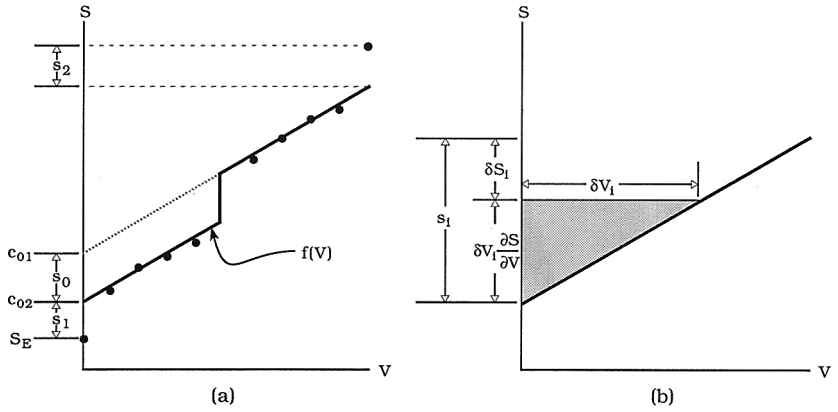

Fig. 4. (a) Pictorial simulation of the S versus V data showing the definitions of the y intercepts (c_{01}, c_{02}) and of the signal shifts (s_0, s_1, s_2). The latter are all positive for shifts in the direction shown. (b) Pictorial representation for the linear dependence of a signal shift s_i on δS_i and δV_i, where $i = 0$, 1, or 2.

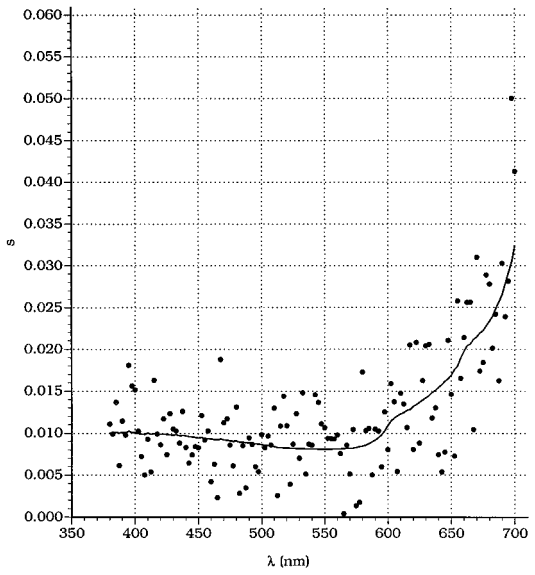

Fig. 6. Net offset s as a function of λ (nanometers). The solid curve is a weighted least-squares fit to the data points; the slight irregularities are due to statistical fluctuations in the $\partial S/\partial V$ data.

dependence on the sample (water) absorption coefficient is obvious. In analogy with Eq. (11), we consider a general function of the form

$$s_0(\lambda) = g_1 + g_2\lambda + (g_3 + g_4\lambda)\frac{\partial S}{\partial V}, \tag{12}$$

where we are assuming a simple linear dependence on wavelength for $\delta S_i \equiv g_1 + g_2\lambda$ and $\delta V_i \equiv g_3 + g_4\lambda$. We do a least-squares fit of Eq. (12) to the $s_0(\lambda)$ data; the required values of $\partial S/\partial V$ at each wavelength have already been obtained from the fits of Eq. (10) to the $S(V)$ data (as in Fig. 3). In this case, the coefficient g_2 is found to be statistically insignificant, so this term is dropped from Eq. (12) and the remaining three terms are again fit to the data. The fitted function is shown as a solid curve in Fig. 5; the values of g_1, g_3, and g_4 are also given together with their standard deviations.

A measurement of an absorbing sample will always consist of first measuring a baseline with the cavity empty, S_E, and then measuring the signal S with the cavity filled. In terms of these and the shifts s_0, s_1, and s_2, our working equation for the ICAM [Eq. (7)] becomes

$$a = \frac{C_1}{4V}(S - S_E - s_0 - s_1 - s_2). \tag{13}$$

Thus, rather than the individual shifts, we require the net offset

$$s(\lambda) = s_0(\lambda) + s_1(\lambda) + s_2(\lambda). \tag{14}$$

One can determine data for the net offset at each wavelength by summing s_0, s_1, and s_2 obtained above or, equivalently, from $s = S(0.6) - S_E - 0.6^*\partial S/\partial V$; Fig. 6 shows $s(\lambda)$. As before, we define the function

$$s(\lambda) = k_1 + k_2\lambda + (k_3 + k_4\lambda)\frac{\partial S}{\partial V} \tag{15}$$

and determine the coefficients k_1, k_2, k_3, and k_4 by a least-squares fit to the $s(\lambda)$ data for $380 \le \lambda \le 700$ nm. The result is the solid curve in Fig. 6; the coefficients, including the covariance matrix, are given in Table 1. The standard deviation of each coefficient is the square root of the corresponding diagonal element of the covariance matrix.[14] Only k_1 and k_2 are required to determine the offset calibration constant C_0''.

Substituting the result of the fit to Eq. (15) into Eq. (13) and using Eq. (8) to replace $\partial S/\partial V$ give

$$a = \frac{C_1}{4V}\left[S - S_E - k_1 - k_2\lambda - \frac{4a}{C_1}(k_3 + k_4\lambda)\right]. \tag{16}$$

Solving for the absorption coefficient a gives the working equation for our present experimental realization of the integrating cavity:

$$a = C_1''(S - S_E - C_0''), \tag{17}$$

where the calibration constants for the normalization and offset are

$$C_1'' = \frac{C_1}{4(V + k_3 + k_4\lambda)}, \tag{18}$$

$$C_0'' = k_1 + k_2\lambda, \tag{19}$$

respectively; both are independent of a, as required. The standard deviation of C_0'' is given by

$$\sigma_{C_0''} = (\sigma_1^2 + \lambda^2\sigma_2^2 + 2\lambda\sigma_{12})^{1/2}, \tag{20}$$

Table 1. Values of the Coefficients and the Corresponding Covariance Matrix for the Least-Squares Fit to the Net Offset $s(\lambda)$

	$k_1 = 1.823 \times 10^{-2}$	$k_2 = 1.841 \times 10^{-5}$	$k_3 = 4.646 \times 10^{-2}$	$k_4 = 8.435 \times 10^{-5}$
	Covariance Matrix			
	k_1	k_2	k_3	k_4
k_1	1.663×10^{-5}	-3.704×10^{-8}	3.336×10^{-5}	-4.170×10^{-8}
k_2	-3.704×10^{-8}	8.501×10^{-11}	-1.039×10^{-7}	1.363×10^{-10}
k_3	3.336×10^{-5}	-1.039×10^{-7}	5.708×10^{-4}	-8.395×10^{-7}
k_4	-4.170×10^{-8}	1.363×10^{-10}	-8.395×10^{-7}	1.242×10^{-9}

where σ_i is the standard deviation of k_i and σ_{12} is the covariance for k_1 and k_2. The constant C_0'' and its standard deviation are evaluated from Eqs. (19) and (20) and Table 1. Determination of the constant C_1'' is discussed in Subsection 4.B. (Note that k_3 and k_4 have been determined, but not C_1.)

B. Determination of the Normalization Calibration Constant C_1''

It is necessary to obtain reference samples of accurately known absorption coefficients. A master dye solution was prepared by dissolving ≈1 mg l^{-1} of Irgalan Black and Alcian Blue in pure water, then filtering this solution through a 0.2-μm Gelman SUPOR-200, membrane filter. The Alcian Blue increases the absorption of the dye solution in the red region of the spectrum so that a uniform, gray absorption spectrum is maintained further into the near infrared; a fairly constant absorption coefficient over the spectral region being studied greatly facilitates determination of the calibration constants as a function of wavelength. The absorption coefficient for the dye in this master solution was measured as a function of wavelength in a Cary 219 spectrophotometer; its uncertainty in the absolute absorption values was less than 1%. (The accuracy of the Cary 219 was verified to within 0.5% with a set of NIST liquid absorption standards.[15]) The master solution was then volumetrically diluted with 1-l volumetric flasks (uncertainty less than 0.1%) and micropipettes (uncertainty less than 1%) to produce 19 reference samples containing concentrations of dye that give absorption coefficients a_{dye} ranging from approximately 0.01 to 8.0 m^{-1}. Adding the uncertainties in quadrature results in an uncertainty of less than 2% in the value of a_{dye} for each reference sample.

For calibration, each of these dye solutions must be measured in the ICAM. However, the output signal of the ICAM for a dye solution is the signal due to the dye plus that due to the pure-water solvent,

$$S_{\text{solution}} = S_{\text{dye}} + S_{\text{pure water}}. \tag{21}$$

From Eq. (17), we have

$$a_{\text{dye}} + a_{\text{pure water}} = C_1''(S_{\text{solution}} - S_E - C_0'') \tag{22}$$

for the dye solutions and

$$a_{\text{pure water}} = C_1''(S_{\text{pure water}} - S_E - C_0'') \tag{23}$$

for the pure-water sample, where S_{solution} and $S_{\text{pure water}}$ are measured ICAM signal outputs. The difference, Eq. (22) minus Eq. (23), gives a calibration equation that relates the measured ICAM signals and the known absorption coefficient a_{dye} of the dye in the reference sample to the unknown calibration constant C_1'':

$$a_{\text{dye}} = C_1''(S_{\text{solution}} - S_{\text{pure water}}) \equiv C_1'' S_{\text{dye}}. \tag{24}$$

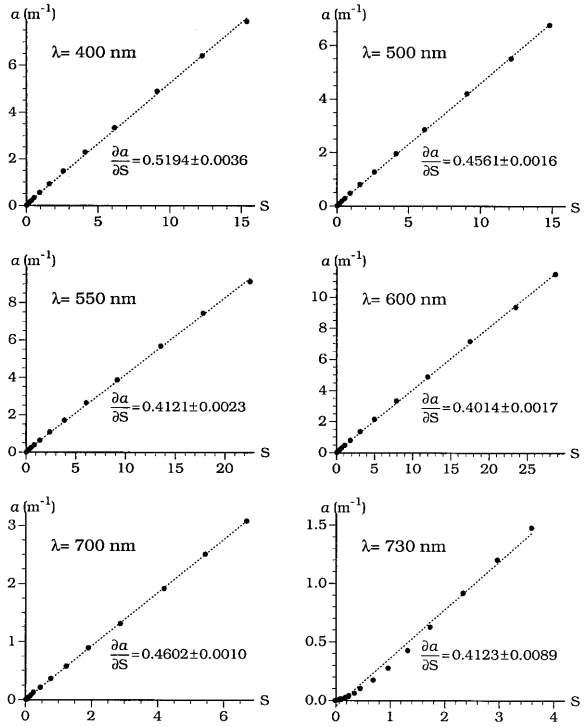

Fig. 7. Examples of the value of the absorption $a \equiv a_{\text{dye}}$ as a function of the observed signal $S \equiv S_{\text{dye}}$ at six wavelengths. Also shown is a straight-line fit to the data together with the corresponding value of the slope and its standard deviation.

Specifically, the calibration constant C_1'', defined in Eq. (18), is given by the slope of the plot of a_{dye} versus S_{dye}:

$$C_1'' = \frac{\partial a_{\text{dye}}}{\partial S_{\text{dye}}}. \tag{25}$$

To implement the calibration, a sample of pure water was placed in the ICAM and $S_{\text{pure water}}$ was measured at 2.5-nm intervals over the wavelength region from 380 to 750 nm. Then the 19 reference samples were sequentially placed in the ICAM in order of increasing dye concentration, and S_{solution} was measured for each at the same wavelengths. Thus 149 spectral measurements were made for each of the 20 samples (19 dye samples and 1 pure-water sample). At each wavelength, the values for the absorption coefficient a_{dye} of the dye in each reference sample were plotted as a function of S_{dye}; the latter is given in terms of the measured signals by $S_{\text{dye}} = S_{\text{solution}} - S_{\text{pure water}}$. A least-squares fit of a straight line (not constrained to pass through the origin) to the data set at each wavelength gives the slope $C_1''(\lambda)$ and its standard deviation; fitted values for $C_1''(\lambda)$ inherently contain the coefficients k_3 and k_4 in the definition in Eq. (18).

Figure 7 shows six examples of these data sets together with the corresponding slopes and standard deviations. For all wavelengths ≤700 nm, a straight line gave an excellent fit to the data. However, for λ ≥ 730 nm the data obviously deviate from a straight

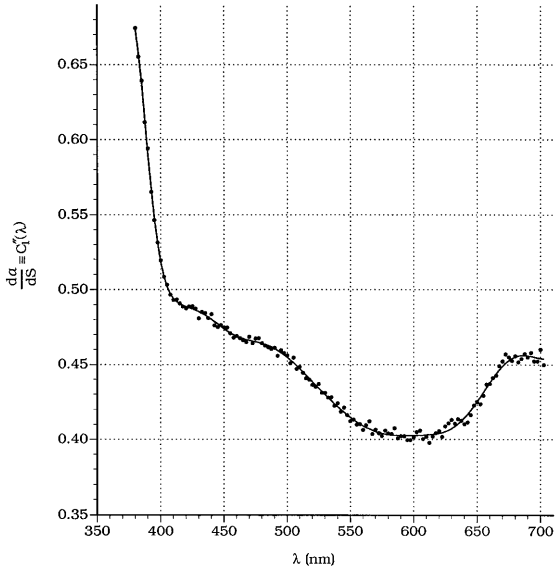

Fig. 8. Observed slopes as a function of wavelength. The solid curve is a least-squares fit to the data by a sum of five Gaussians.

line as can be seen from the last of the examples in Fig. 7. Because of the nonlinearity, the measurements for $\lambda \geq 700$ nm were not used in the determination of either C_1'' or C_0''. In the transition region, 700–720 nm, the straight-line fits are visually quite good; as the wavelength increases, the first statistical evidence of a problem is a persistent increase in the standard deviation of the fitted slope beginning at ≈715 nm. The choice of an upper limit of 700 nm for the data to be used in the analysis is somewhat arbitrary but does ensure that the nonlinear effects appear well outside the region of study. The source of the nonlinearity was not investigated.

The values of C_1'' as a function of wavelength are shown in Fig. 8. The solid curve is a least-squares fit of these data to a sum of five Gaussians:

$$C_1''(\lambda) = a_1 + \sum_{i=1}^{5} a_{3i-1} \exp\left(\frac{\lambda - a_{3i}}{a_{3i+1}}\right)^2, \qquad (26)$$

which contains 16 fitting parameters a_i. They were determined by using the least-squares fitting program, PRO FIT[16]; their values and standard deviations are given in Table 2. Based on the magnitudes and standard deviations of their amplitudes, the two Gaussians with amplitudes a_2 and a_8 dominate the fit. The standard deviation of C_1'' is

$$\sigma_{C_1''} = \left[\sum_{i=1}^{16}\left(\frac{\partial C_1''}{\partial a_i}\right)^2 \sigma_i^{\,2} + 2\sum_{i=1}^{16}\sum_{j=i+1}^{16}\left(\frac{\partial C_1''}{\partial a_i}\right)\left(\frac{\partial C_1''}{\partial a_j}\right)\sigma_{ij}\right]^{1/2}, \qquad (27)$$

where σ_i is the standard deviation of a_i, and σ_{ij} is the covariance for a_i and a_j. The calibration constant $C_1''(\lambda)$ can be evaluated with Eq. (26) and the data in Table 2. The derivatives of C_1'' required for the evaluation of $\sigma_{C_1''}$ can be determined directly from Eq. (26); the required covariances are provided by the PRO FIT routines but are not listed here. The values of

Table 2. Values of the Coefficients and Their Standard Deviations for the Least-Squares Fit of the Sum of Five Gaussians, Eq. (26), to the $da/dS \equiv C_1''$ Data[a]

	Amplitude		Gaussian Center (nm)		Gaussian Width σ (nm)
a_1	0.4919 ± 0.0020		—		—
a_2	0.1934 ± 0.0079	a_3	375.7 ± 1.1	a_4	17.4 ± 0.9
a_5	−0.0108 ± 0.0018	a_6	459.7 ± 2.5	a_7	24.6 ± 4.8
a_8	−0.0876 ± 0.0035	a_9	580.6 ± 6.3	a_{10}	85.8 ± 7.4
a_{11}	−0.0234 ± 0.0107	a_{12}	639.0 ± 2.1	a_{13}	33.5 ± 7.3
a_{14}	−0.0281 ± 0.0048	a_{15}	710.7 ± 2.3	a_{16}	28.3 ± 4.0

[a] Each row gives the three coefficients for one of the Gaussians: amplitude, center, and width.

$\sigma_{C_1''}$ increase from ≈0.003 at 380 nm to ≈0.01 at 700 nm.

To summarize, the two calibration constants $C_0''(\lambda)$, $C_1''(\lambda)$ required by the ICAM working equation [Eq. (17)] are shown in Fig. 9.

C. Relative Calibration

Although not applicable to the water absorption measurements, we emphasize that only $C_1''(\lambda)$ is necessary for making relative absorption measurements. For example, for the measurement of the absorption of particles in a liquid suspension, the relevant working equation is given in analogy with Eq. (24) by

$$a_{\text{particulates}} = C_1''(S_{\text{suspension}} - S_{\text{liquid}}). \qquad (28)$$

In a practical implementation, one would (a) measure the ICAM signal for the suspension; (b) pass the suspension through a fine filter to remove the particles; (c) measure the ICAM signal for the liquid filtrate; and (d) subtract the two ICAM signals and multiply by $C_1''(\lambda)$ from Eq. (26) to obtain $a_{\text{particulates}}$.[8]

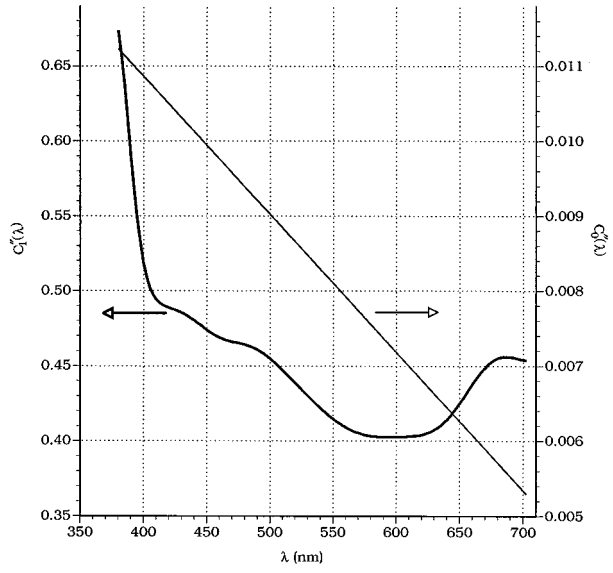

Fig. 9. Wavelength dependence of the two calibration constants.

Table 3. Absorption Coefficients, a_w, and Standard Deviations σ, for Pure Water as a Function of Wavelength λ[a]

λ (nm)	a_w (m^{-1})	σ (m^{-1})	Percent
380.0	0.01137	0.0016	14
382.5	0.01044	0.0015	15
385.0	0.00941	0.0011	13
387.5	0.00917	0.0014	16
390.0	0.00851	0.0012	15
392.5	0.00829	0.0011	14
395.0	0.00813	0.0010	13
397.5	0.00775	0.0011	15
400.0	0.00663	0.0007	11
402.5	0.00579	0.0007	12
405.0	0.00530	0.0007	14
407.5	0.00503	0.0006	13
410.0	0.00473	0.0006	13
412.5	0.00452	0.0005	13
415.0	0.00444	0.0006	13
417.5	0.00442	0.0006	14
420.0	0.00454	0.0006	14
422.5	0.00474	0.0006	13
425.0	0.00478	0.0006	14
427.5	0.00482	0.0006	13
430.0	0.00495	0.0006	12
432.5	0.00504	0.0005	11
435.0	0.00530	0.0005	11
437.5	0.00580	0.0005	10
440.0	0.00635	0.0005	9
442.5	0.00696	0.0005	9
445.0	0.00751	0.0006	8
447.5	0.00830	0.0005	7
450.0	0.00922	0.0005	6
452.5	0.00969	0.0004	6
455.0	0.00962	0.0004	5
457.5	0.00957	0.0004	5
460.0	0.00979	0.0005	6
462.5	0.01005	0.0005	6
465.0	0.01011	0.0006	7
467.5	0.0102	0.0006	6
470.0	0.0106	0.0005	6
472.5	0.0109	0.0008	8
475.0	0.0114	0.0007	7
477.5	0.0121	0.0008	8
480.0	0.0127	0.0008	7
482.5	0.0131	0.0008	7
485.0	0.0136	0.0007	6
487.5	0.0144	0.0007	6
490.0	0.0150	0.0007	5
492.5	0.0162	0.0014	9
495.0	0.0173	0.0010	6
497.5	0.0191	0.0014	8
500.0	0.0204	0.0011	6
502.5	0.0228	0.0012	6
505.0	0.0256	0.0013	6
507.5	0.0280	0.0010	5
510.0	0.0325	0.0011	4
512.5	0.0372	0.0012	4
515.0	0.0396	0.0012	4
517.5	0.0399	0.0015	5
520.0	0.0409	0.0009	3
522.5	0.0416	0.0014	4
525.0	0.0417	0.0010	4
527.5	0.0428	0.0017	5
530.0	0.0434	0.0011	4
532.5	0.0447	0.0017	5
535.0	0.0452	0.0012	4
537.5	0.0466	0.0015	4
540.0	0.0474	0.0010	3
542.5	0.0489	0.0016	4
545.0	0.0511	0.0011	3
547.5	0.0537	0.0016	4
550.0	0.0565	0.0011	3
552.5	0.0593	0.0012	3
555.0	0.0596	0.0012	3
557.5	0.0606	0.0014	4
560.0	0.0619	0.0010	3
562.5	0.0640	0.0015	4
565.0	0.0642	0.0009	3
567.5	0.0672	0.0014	3
570.0	0.0695	0.0011	3
572.5	0.0733	0.0017	4
575.0	0.0772	0.0011	3
577.5	0.0836	0.0016	3
580.0	0.0896	0.0012	3
582.5	0.0989	0.0016	3
585.0	0.1100	0.0012	3
587.5	0.1220	0.0018	3
590.0	0.1351	0.0012	3
592.5	0.1516	0.0017	3
595.0	0.1672	0.0014	3
597.5	0.1925	0.0019	3
600.0	0.2224	0.0017	3
602.5	0.2470	0.0023	3
605.0	0.2577	0.0019	3
607.5	0.2629	0.0028	3
610.0	0.2644	0.0019	3
612.5	0.2665	0.0023	3
615.0	0.2678	0.0019	3
617.5	0.2707	0.0026	3
620.0	0.2755	0.0025	3
622.5	0.2810	0.0039	3
625.0	0.2834	0.0028	3
627.5	0.2904	0.0039	3
630.0	0.2916	0.0027	3
632.5	0.2995	0.0038	3
635.0	0.3012	0.0028	3
637.5	0.3077	0.0049	3
640.0	0.3108	0.0028	3
642.5	0.322	0.005	3
645.0	0.325	0.003	3
647.5	0.335	0.004	3
650.0	0.340	0.003	3
652.5	0.358	0.006	3
655.0	0.371	0.003	3
657.5	0.393	0.006	3
660.0	0.410	0.004	3
662.5	0.424	0.005	3
665.0	0.429	0.004	3
667.5	0.436	0.005	3
670.0	0.439	0.004	3
672.5	0.448	0.007	3
675.0	0.448	0.004	3
677.5	0.461	0.006	3
680.0	0.465	0.004	3
682.5	0.478	0.006	3
685.0	0.486	0.004	3
687.5	0.502	0.006	3
690.0	0.516	0.004	3
692.5	0.538	0.007	3

Continued on following page.

Table 3. *Continued.*

λ (nm)	a_w (m^{-1})	σ (m^{-1})	Percent
695.0	0.559	0.005	3
697.5	0.592	0.008	3
700.0	0.624	0.006	3
702.5	0.663	0.008	3
705.0	0.704	0.006	3
707.5	0.756	0.009	3
710.0	0.827	0.007	3
712.5	0.914	0.011	3
715.0	1.007	0.009	3
717.5	1.119	0.014	3
720.0	1.231	0.011	3
722.5	1.356	0.008	3
725.0	1.489	0.006	3
727.5	1.678	0.007	3

[a]Percent error is based on σ as well as estimates of systematic errors. Spectral resolution: 2.5 nm ($490 < \lambda < 730$ nm); 5 nm ($380 \le \lambda < 400$ nm, $470 < \lambda \le 490$ nm); 7 nm ($400 \le \lambda \le 470$ nm).

Similarly, for a solute dissolved in a solvent to produce a solution, the relevant working equation is

$$a_{\text{solute}} = C_1''(S_{\text{solution}} - S_{\text{solvent}}), \tag{29}$$

where, for example, in the case of dissolved organic matter the solvent would be pure water.[8]

5. Pure Water

Water triply distilled in quartz has been previously accepted as pure; however, some organics with low boiling points will not be efficiently removed by this method.[17] Reagent-grade water, Type I, is the purest category defined by standard specifications. This high-purity water will leach contamination from its environment.[17] We used Type I water from Culligan and Millipore commercial water purification systems; both supplied water with electrical resistivity of ≈18 MΩ cm. The Millipore system was the one used in the measurements of the previous paper and is described there in greater detail.[3] When preparing for pure-water measurements, all glassware, the ICAM sample cavity, and ICAM inlet tubing were thoroughly washed with a potassium-dichromate and sulfuric acid solution, rinsed by flowing 15 l of pure Type I water through the system, and then purged with dry nitrogen prior to the measurement sequence. The pure-water delivery systems were purged by drawing 2–3 l of pure water from the system prior to obtaining samples for measurement. This was done to remove any bacterial contamination in the lines. Storage and transport containers were thoroughly rinsed with pure Type I water prior to drawing the measurement sample. Samples were taken directly from the delivery system to the ICAM laboratory and measured immediately.

6. Absorption Data and Error Discussion

Since the nominal bandwidth of the monochromator was ~2 nm, data were taken at wavelength intervals of 2.5 nm. Water from both the Culligan and Millipore commercial water purification systems was measured by the ICAM. Since the difference between common data points in the two sets was always less than the larger of 3% or 0.0018 m^{-1}, averaging data from the two sets is appropriate. In every case, a weighted average is used in which the weighting factor for each point is the reciprocal of its variance.

Furthermore, prior to averaging of the data sets, the statistical fluctuations in the 380–490-nm region were partially smoothed by averaging over adjacent wavelength intervals with a binomial distribution spanning three intervals,[14] while also weighting each point with the reciprocal of its variance. Thus the smoothing algorithm is

$$a_i' = \frac{a_{i-1}/\sigma_{i-1}^2 + 2a_i/\sigma_i^2 + a_{i+1}/\sigma_{i+1}^2}{1/\sigma_{i-1}^2 + 2/\sigma_i^2 + 1/\sigma_{i+1}^2}, \tag{30}$$

where a_i is the original absorption coefficient for wavelength interval i and σ_i is its standard deviation. The standard deviation for the new absorption value a_i' is

$$\sigma_{a_i'} = \frac{(1/\sigma_{i-1}^2 + 4/\sigma_i^2 + 1/\sigma_{i+1}^2)^{1/2}}{1/\sigma_{i-1}^2 + 2/\sigma_i^2 + 1/\sigma_{i+1}^2}. \tag{31}$$

The cost of this smoothing is a decrease in the spectral resolution from 2.5 to 5 nm for the data in this spectral region. Finally, after averaging the data sets, the smoothing algorithm [Eq. (30)] was applied once more to the data in the 400–470-nm region. The spectral resolution for these data is thus further reduced to ≈7 nm.

The final results[18] are tabulated in Table 3; at each wavelength, values are given for the absorption coefficient, its statistical standard deviation, and the percent error. The statistical standard deviations are tracked from the initial voltage measurements and include the standard deviations of the parameters in the smooth calibration functions; since the ICAM signal is quite stable, the standard deviations are generally small. We estimated the percent error by adding the statistical standard deviation in quadrature with the error in the absolute value of the absorption coefficient for the calibration reference samples (estimated at 2% in the first paragraph of Subsection 4.B); the value quoted in Table 3 for the percent error was obtained by rounding up to an integer percentage.

No error is included for the temperature that had peak variations of less than ±1 °C. However, for such variations, the errors associated with absorption measurements in the red should be generally negligible (e.g., extremes of less than ±0.7% at 600 nm).[19] There are also hints of temperature-dependent changes in a at 515 nm and possibly 550 nm.[19] If they are as large as $+0.003\ m^{-}\ °C^{-1}$ as suggested by Højerslev and Trabjerg,[20] they could be appreciable in the blue. The final resulting errors quoted in Table 3 are generally quite small; however, aside from effects that are due to small possible temperature variations, their estimation has been consistently

kept conservative. If there are any other systematic errors, their origin is currently unknown.

The final results are shown in Fig. 10 for comparison with the results of Sogandares and Fry,[3] Buiteveld *et al.*,[2] Smith and Baker,[6] and Tam and Patel[4]; they are in excellent agreement with each of these other four over at least some part of the spectrum. The present results show the seventh and eighth harmonics of the O–H stretch and the minimum at ≈420 nm that were first observed by Sogandares and Fry. The minimum observed in the present data is lower, and, although it is by an amount whose statistical significance is marginal, there are two possible explanations: (1) The Sogandares and Fry experiment was an extremely difficult *tour de force* and as such was vulnerable to systematic effects. (2) In the present experiment, the temperature of the water sample was 22 °C, whereas in the Sogandares and Fry experiment, it was actively stabilized at a higher temperature of 25.0 ± 0.1 °C (above room temperature). Such a temperature increase would be expected to increase a slightly.[19,20]

In the case of the Smith and Baker (S&B) data, there is significant disagreement below 490 nm. This disagreement is most likely due to a combination of (1) our more effective water purification and maintenance, (2) the absence of scattering effects in the ICAM, and (3) the greater sensitivity of the ICAM.

At first glance, there seems to be a striking disagreement with the results given by Buiteveld *et al.*[2] for wavelengths below 500 nm. However, Buiteveld *et al.* values in the 300–394-nm wavelength range were obtained from the total attenuation coefficients measured by Boivin *et al.*[21] by subtracting estimates of the scattering contributions. The uncertainty in the attenuation coefficients is given by Boivin *et al.* to be $\pm 0.007\ \mathrm{m}^{-1}$; thus the uncertainty in the absorption coefficient must be even greater. This uncertainty exceeds the value of the absorption coefficient in the region of the minimum. Furthermore, in the 394–520-nm wavelength range, Buiteveld *et al.* use the Smith and Baker data shifted by an amount that matches the value they obtained from the Boivin *et al.* results at 394 nm; these data therefore also pick up similar errors. In summary, the uncertainties in the Buiteveld *et al.* results are so large that they are, in fact, in complete agreement with our results throughout the blue and ultraviolet.

The disagreement with the Tam and Patel data is most striking below 490 nm. This is unquestionably a result of contamination by their stainless steel cell. For example, at 425 nm we even observe an increase in a of $\approx 0.0006\ \mathrm{m}^{-1}\ \mathrm{day}^{-1}$ for a pure-water sample stored in clean Pyrex. In the presence of metal, the increase in the blue absorption can be disastrous; pure water is a hungry substance that leaches impurities out of nearly everything it contacts.[17]

Finally, there is a useful internal consistency check. From Eqs. (8) and (9), we have for an ideal ICAM

$$a = V \left.\frac{\partial a}{\partial S}\right|_V \left.\frac{\partial S}{\partial V}\right|_a , \tag{32}$$

where a is the absorption coefficient of the sample for which $\partial S/\partial V$ is measured, and V is the volume of the sample for which $\partial a/\partial S$ is measured. Of course, Eq. (32) does not directly apply to our practical experimental realization of the ICAM. Using Eqs. (17) and (18), we find

$$\left.\frac{\partial a}{\partial S}\right|_V = \frac{C_1}{4(V + k_3 + k_4\lambda)} , \tag{33}$$

which is the generalization of Eq. (9) from an ideal ICAM to our experimental realization of it. Solving Eq. (8) for C_1, substituting in Eq. (33), and then solving for a give

$$a = (V + k_3 + k_4\lambda) \left.\frac{\partial a}{\partial S}\right|_V \left.\frac{\partial S}{\partial V}\right|_a , \tag{34}$$

which is the generalization of Eq. (32) to our real cavity. Physically, Eq. (34) states that the perturbation of the radiance distribution in our experimental realization of the cavity results in an effective sample volume slightly different from the actual sample volume.

We emphasize that Eq. (34) provides an essentially independent measurement of a. Specifically, in this case, most of the absorption coefficient information is contained in the $\partial S/\partial V$ data. In the previous analysis for the two ICAM calibration constants $C_0''(\lambda)$ and $C_1''(\lambda)$, the only use of the $\partial S/\partial V$ data was to

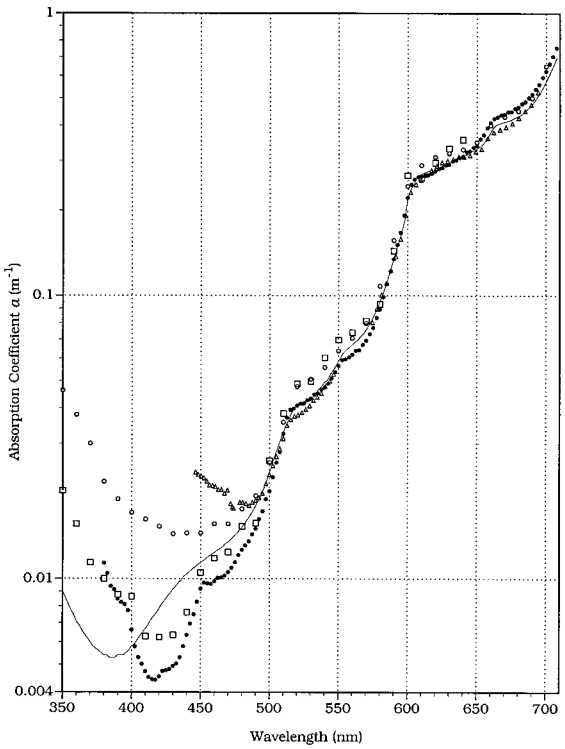

Fig. 10. Present results (●) for the absorption of pure water plotted with those from Buiteveld *et al.*[2] (smooth curve), Tam and Patel[4] (△), Smith and Baker[6] (○), and Sogandares and Fry[3] (□).

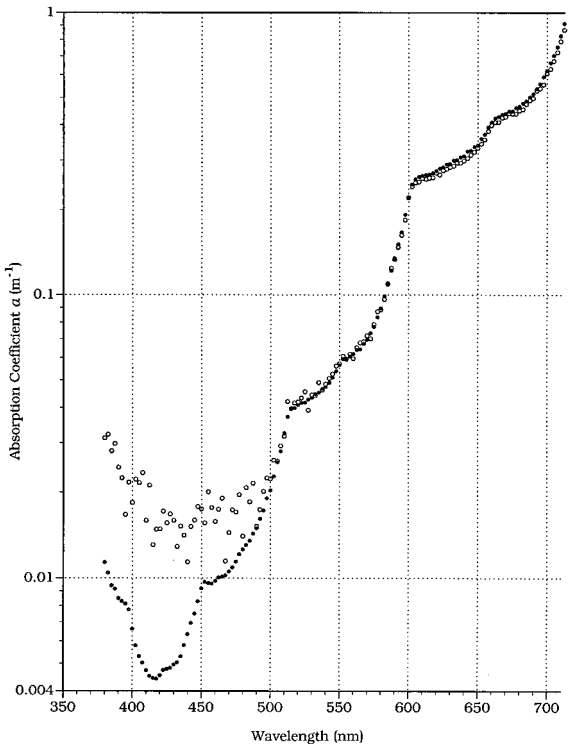

Fig. 11. Comparison of our final results given in Table 3 (●) with those obtained from Eq. (34) (○).

extract the constants k_1, k_2, k_3, and k_4 from a fit to the $s(\lambda)$ data. However, the coefficients, k_3 and k_4, of $\partial S/\partial V$ in the fit were not even used; only k_1 and k_2 were required to determine $C_0''(\lambda)$. Furthermore, $C_0''(\lambda)$ produces a relatively small correction to measured values of S [compare S to $C_0''(\lambda)$ in Figs. 3 and 9, respectively].

By using k_3 and k_4 from Table 1, we evaluated a from Eq. (34); results are shown in Fig. 11 together with our data from Table 3. The disagreement below 500 nm is expected since the time-consuming $\partial S/\partial V$ measurements were not compatible with the use and maintenance of high water purity; the spectrum in this region is typical of that for pure water after it has been stored in Pyrex for several days. The excellent agreement over the rest of the spectrum demonstrates the internal consistency of the data and provides a convincing argument for the validity of the ICAM instrumentation and of our analysis. The data above 600 nm does appear to be systematically low by ≈3%. The origin of this systematic shift is in the volume factor, $V + k_3 + k_4\lambda$, of Eq. (34); its standard deviation is ≈2.5% in the 600–700-nm range (from Table 1 and assuming $\sigma_v \approx 1\%$). For example, increasing k_4 by just one standard deviation from its fitted value (8.44×10^{-5} to 11.96×10^{-5}) eliminates the discrepancy.

7. Resonance Structures

Table 4 summarizes the positions of some predicted shoulders and peaks in the absorption spectra of pure water. The vibrational mode assignments in Table 4 indicate the order of the harmonic of the O–H stretch mode (ν_1/ν_3) or scissors mode (ν_2). All boldface entries refer to harmonics of the O–H stretch mode; their predicted frequencies are based

Table 4. Mode Assignments with the Predicted Frequencies and Wavelengths[a]

Mode Assignments		Predicted Shoulder Frequencies	Predicted Shoulder Wavelengths
ν_1/ν_3	ν_2	ν (cm^{-1})	λ (nm)
1	**0**	**3557**	**2811**
0	1	1645	6079
4	**0**	**13472**	**742**
4	1	15117	662
5	**0**	**16525**	**605**
5	1	18170	550
6	**0**	**19452**	**514**
6	1	21097	474
7	**0**	**22253**	**449**
7	1	23898	418
8	**0**	**24928**	**401**
8	1	26573	376

[a]For the harmonics of the O–H stretch given by Eq. (34) (in boldface) and for combination modes of the harmonics of the O–H stretch with the fundamental of the scissors mode (in lightface type).

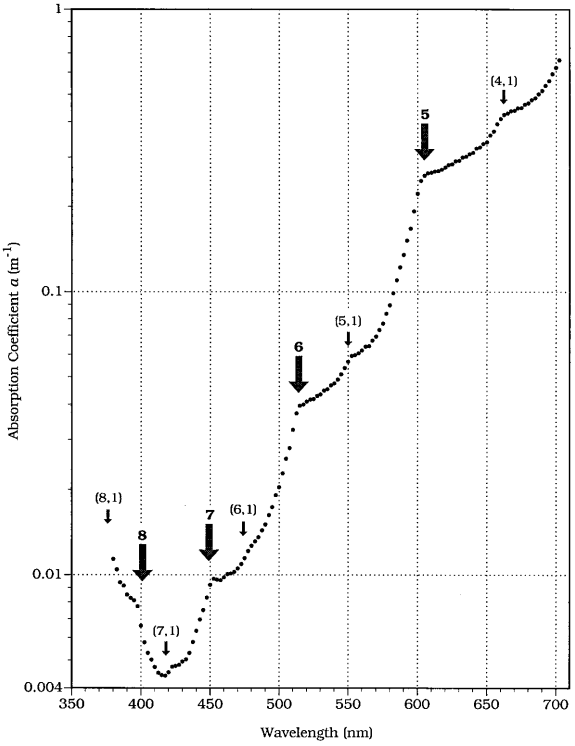

Fig. 12. Present results for the absorption of pure water. A large arrow with a boldface integer **n** indicates the predicted position of a shoulder that is due to the nth harmonic of the O–H stretch; the small arrows with mode assignments (j, 1) indicate the predicted position of a combination of the jth harmonic of the O–H stretch with the fundamental of the scissors mode.

on the simple anharmonic formula given by Tam and Patel[4]:

$$\nu_n = n(3620 - 63n)\text{cm}^{-1}. \quad (35)$$

Lightface type in Table 4 refers to combinations of the fundamental scissors mode with harmonics of the stretch mode. We obtained the predicted frequencies of these combination modes by adding the fundamental frequency of the scissors mode, $\nu_2 = 1645$ cm^{-1} (Ref. 22), to the harmonic frequencies of the stretch mode.

The resolution of the ICAM accentuates subtle structure that has not been readily apparent in other water absorption data. Figure 12 is another plot of our data to emphasize this structure. Each large arrow, labeled with a boldface integer **n**, shows the predicted position of a shoulder that is due to the nth harmonic of the fundamental O–H stretching mode. The shoulders that are due to the seventh and eighth harmonics were first observed by Sogandares and Fry,[3] but they are much more clearly defined here. The position of the eighth harmonic shoulder appears to be at a wavelength ≈5 nm shorter than that predicted in Table 4.

We have made the first observations of a minor shoulder between major shoulders. These minor shoulders are interpreted as combination modes in which harmonics of the O–H stretch are combined with the fundamental of the scissors mode. The predictions for the wavelengths of these combination modes are given in Table 4 and are indicated in Fig. 12 by the small arrows; the pair of numbers in parentheses above each small arrow indicate the mode assignments (ν_1/ν_3, ν_2). The close match of the positions of the small arrows to the positions of the minor shoulders provides the basis for our conclusion.

The (8, 1) combination mode is outside the measurement region for this study, and the (6, 1) mode is barely visible, but the others are obvious. The reader is cautioned not to read anything into the fluctuations at 460 nm. Specifically, the data for water from the Millipore system were relatively smooth over this region to the edge of the seventh-harmonic shoulder, whereas the data set for water from the Culligan system appears to have some noise spikes here that lead to the irregularities in the final average of the data from these two sources. The minor shoulder at ≈420 nm and the slight bump at ≈476 nm could be identified in both sets before they were averaged together. Of course, noise on the data is always much more obvious in flat parts of a spectrum than on steeply varying parts.

8. Summary

The operation and analysis of the ICAM for the measurement of weak optical absorption to high absolute accuracy has been demonstrated. We believe we are providing the most reliable data available for the absorption coefficient of pure water at 22 °C over the 380–700-nm spectral range. We have confirmed the seventh and eighth harmonics of the O–H stretch. Finally, we have made the first observations of the combination mode between the fundamental frequency of the scissors motion and harmonics of the O–H stretch.

We gratefully acknowledge support from the Welch Foundation under grant A-1218, from the Texas Advanced Technology Program grant 10366-16, and from the Office of Naval Research grant N00014-96-1-0410. This research was part of R. M. Pope's dissertation requirement in the Physics Department, Texas A&M University, 1993. We thank Marvin Blizard for helpful suggestions and encouragement in the early development of this concept; Shifang Li who actively participated in the initial efforts; Alan Wiedemann and Scott Pegau for enlightening discussions and comments; Thomas Walther and Yves Emery for critically reading the manuscript. Finally, the enthusiasm, encouragement, and expertise of George Kattawar were invaluable to the success of this project.

References and Notes

1. M. R. Querry, D. M. Wieliczka, and D. J. Segelstein, "Water (H_2O)," in *Handbook of Optical Constants of Solids II*, E. D. Palik, ed., (Academic, San Diego, Calif., 1991), pp. 1059–1077.
2. H. Buiteveld, J. H. M. Hakvoort, and M. Donze, "The optical properties of pure water," in *Ocean Optics XII*, J. S. Jaffe, ed., Proc. SPIE **2258,** 174–183 (1994).
3. F. M. Sogandares and E. S. Fry, "Absorption spectrum (340–640 nm) of pure water. I. photothermal measurements," Appl. Opt. **36,** 8699–8709 (1997).
4. A. C. Tam and C. K. N. Patel, "Optical absorptions of light and heavy water by laser optoacoustic spectroscopy," Appl. Opt. **18,** 3348–3358 (1979).
5. E. S. Fry, G. W. Kattawar, and R. M. Pope, "Integrating cavity absorption meter," Appl. Opt. **31,** 2055–2065 (1992).
6. R. C. Smith and K. S. Baker, "Optical properties of the clearest natural waters (200–800 nm)," Appl. Opt. **20,** 177–184 (1981).
7. F. M. Sogandares, "The spectral absorption of pure water," Ph.D. dissertation (Texas A&M University, College Station, Tex., 1991).
8. R. M. Pope, "Optical absorption of pure water and sea water using the integrating cavity absorption meter," Ph.D. dissertation (Texas A&M University, College Station, Tex., 1993).
9. Xenon Arc-Lamp Model 66005 (Oriel Corporation, Stratford, Conn.).
10. Monochromator, Digikrom Model 240 (CVI Laser Corporation, Albuquerque, N.M.).
11. Electromagnetic Camera Shutter (Copal Model DC495, R.T.S., Inc., Deer Park, N.Y.).
12. High diffuse reflectance material, Spectralon SRM-99 (Labsphere, Inc., North Sutton, N.H.).
13. See Section IX of Ref. 5.
14. P. R. Bevington and D. K. Robinson, *Data Reduction and Error Analysis for the Physical Sciences*, 2nd ed. (McGraw-Hill, New York, 1969).
15. The liquid absorption standards are identified by NBS#931d, Lot#680312, and were obtained from the NIST Office of Standard Reference Materials.
16. A software program for the MacIntosh, PRO FIT (QuantumSoft, Cherwell Scientific, Oxford, 1996).
17. "Ultrapure ion free/organic free water for trace analysis," Lit. No. CG302 (Millipore Corporation Bedford, Mass., 1986).
18. Note that although exactly the same raw data were used, the values quoted here are different from those in Pope's disser-

tation,[8] which contains a systematic error that is due to a dependence of one calibration constant on the water absorption coefficient (his Fig. V-8). The thorough analysis leading to our Eqs. (18) and (19) avoids this problem; also, we have used rigorous statistically averaging techniques to extract the maximum information from the raw data.
19. W. S. Pegau and J. R. V. Zaneveld, "Temperature-dependent absorption of water in the red and near-infrared portions of the spectrum," Limnol. Oceanogr. **38,** 188–192 (1993).
20. N. K. Højerslev and I. Trabjerg, "A new perspective for remote measurements of plankton pigments and water quality," Rep. No. 51 (Københavns Universitet Geofysisk Institut, Copenhagen, Denmark, 1990).
21. L. P. Boivin, W. F. Davidson, R. S. Storey, D. Sinclair, and E. D. Earle, "Determination of the attenuation coefficients of visible and ultraviolet radiation in heavy water," Appl. Opt. **25,** 877–882 (1986).
22. J. G. Bayly, V. B. Kartha, and W. H. Stevens, "The absorption spectra of liquid phase H_2O, HDO, and D_2O from 0.7 μm to 10 μm," Infrared Phys. **3,** 211–223 (1963).